JOURNAL OF AIRCRAFT
Vol. 47, No. 6, November–December 2010

Dynamic Sensitivity to Atmospheric Turbulence of Unmanned Air Vehicles with Varying Configuration

Mujahid Abdulrahim*
University of Florida, Gainesville, Florida 32611
Simon Watkins,† Reuven Segal,‡ and Matthew Marino‡
RMIT University, Melbourne, Victoria 3001, Australia
and
John Sheridan†
Monash University, Melbourne, Victoria 3800, Australia

DOI: 10.2514/1.46860

Air vehicle flight in turbulence is generally treated as an anomalous part of the flying environment. Aircraft geometries and flight-control systems are often designed and tested for calm atmospheric conditions, where both steady winds and gusts are minor. As a result, the flight performance of small aircraft deteriorates in the presence of atmospheric turbulence, where gust disturbances can be large relative to the flying speeds. A better approach is needed in the aircraft and control system design process that specifically accounts for the effects of turbulence and provides a means of mitigating disturbances to improve the mission effectiveness of micro unmanned air vehicles and small unmanned air vehicles. The current research considers untethered flight tests of a small unmanned air vehicle in a large wind engineering tunnel that can be configured to replicate turbulence levels expected from urban and suburban environments. Systematic changes to the configuration of the fixed-wing aircraft are made to evaluate the role of metrics, such as c.g., mass, moment of inertia, wingspan, and wing loading to turbulence sensitivity. Estimates of the force and moment disturbances indicate that some parameters, such as moment of inertia, have simple and expected influences on the response to turbulence. Conversely, wing area and mass have conflicting effects due to the compounded influences on the aircraft response. The sensitivity of the various aircraft configurations to turbulence are presented as control equivalent turbulence disturbances, which equate forces and moments acting on the airframe to control deflections. This method normalizes the aircraft responses with respect to the ability to suppress disturbances with actuated controls.

Nomenclature

A	=	system dynamics
a_y	=	lateral acceleration
a_z	=	vertical acceleration
B	=	control effectiveness
b	=	wingspan
C	=	state observation
c	=	wing chord
E	=	disturbance dynamics
F	=	fit quality
$I_{x,y,z}$	=	moments of inertia
I_{xz}	=	product of inertia
l	=	rolling moment
m	=	pitching moment
n	=	yawing moment
p	=	roll rate
q	=	pitch rate
$\bar{q}$	=	dynamic pressure
r	=	yaw rate
S	=	wing area
u, δ	=	control input
V_0	=	velocity
x	=	state vector
Y	=	side force
y	=	measurements
Z	=	vertical force
α	=	angle of attack
β	=	angle of sideslip

Subscripts

d	=	disturbance force/moment
lat	=	lateral
lon	=	longitudinal
T	=	total force/moment contributions
a	=	aircraft-only force/moment contributions
δ_a	=	aileron
δ_e	=	elevator
δ_r	=	rudder

Presented as Paper 2009-5907 at the AIAA Guidance, Navigation, and Control Conference, Chicago, IL, 10–13 August 2009; received 25 August 2009; revision received 7 August 2010; accepted for publication 10 August 2010.

*Research Associate; mujahid@ufl.edu. Member AIAA.
†Professor. Member AIAA.
‡Postgraduate student. Student Member AIAA.

I. Introduction

THE role of a micro air vehicle (MAV) or unmanned air vehicle (UAV) is generally one of reconnaissance using visual, audio, chemical, or radiological sensors. The fundamental flight requirement is effective sensor placement, a task which is expected to involve maneuvering around and possibly inside urban obstacles. Wind flowing around such obstacles generates turbulence, which can be of significant intensity relative to the mean flying speed of MAVs. It is the flight of MAVs in turbulence that puts into question the success of missions for which the aircraft are designed.

The low mass and slow flying speed of MAVs and small UAVs exacerbates the influence of turbulence on the flight path. Relative to manned aircraft, MAVs sustain extreme levels of turbulence due to the scaling effects of mass and speed [1]. Sensitivity to turbulence must be a conscious factor in the design of MAV airframes and

Fig. 1 Flight tests of the variable-configuration UAV in calm-wind open-air flight (configuration 2a, left) and in the turbulent wind tunnel (configuration 3a, right). See Table 1 for configuration details.

control systems. Some MAV designs use flexible wing structures as a method of passive disturbance alleviation [2], while others have employed movable wing segments to dynamically vary the lift distribution and reduce responses to turbulence. Other strategies focus on distributed actuation [3] or control designs insensitive to disturbances [4] to mitigate the effect of turbulence. In many cases, the vehicle designs and control systems are tested and tuned in calm-wind open-atmosphere flight, away from turbulence-inducing landscape features. When turbulence is present during tests, the flow is rarely well documented, causing ambiguity in the nature of the disturbances against which the vehicle systems are intended to act.

The current paper presents results from a series of systematic experiments in which vehicle configuration is changed and flown untethered in a wind tunnel with measured turbulence levels. Turbulence length scale and intensity are controlled by the tunnel configuration, resulting in continuous, mixed turbulent flow having consistent statistical properties. The tunnel is large enough to permit flight of large MAVs (or small UAVs) in one of several test sections. Aircraft are tested with variations to fundamental design parameters to determine the corresponding influence on handling qualities in the presence of turbulence. The aircraft are also flown in identical configurations in open-atmosphere testing to determine disparities in flying characteristics between the different environments, shown in Fig. 1. In both the wind-tunnel and open-atmosphere flight tests, a pilot manually manipulates the control surfaces using a remote transmitter to fly the aircraft. The wind-tunnel tests consist of straight-and-level flight near the center of the test section.

Section II gives an overview of the wind tunnel, aircraft, modified configurations, and experimental process. Section III describes flight-test experiments, which include both the outdoor flight tests for dynamic modeling and the wind-tunnel flight tests. Section IV presents a simple method for estimating the forces and moments imparted on the aircraft from the turbulence. The wind-tunnel responses are compared with predicted responses using the dynamics identified from the flight test and the pilot inputs from the wind-tunnel tests. The paper concludes with some remarks on using anticipated aircraft performance in turbulence as a fundamental trade during the preliminary design process.

II. Background and Overview

This research investigates the effect of configuration changes on open-air and turbulent-tunnel flight-test results of a fixed-wing aircraft. Figure 2 shows the aircraft used in the flight experiments. The foam fixed-wing aircraft is a commercially available recreational model aircraft. Modifications made to the aircraft allow parametric changes to the span, wing loading, mass, moment of inertia, and center of gravity.

A. Wind Tunnel

Flight trials are conducted in the Monash University wind engineering tunnel. The facility is the largest wind tunnel in the southern hemisphere and has three test sections suitable for MAV flight. The upper level in particular has a cross section 12 m wide and 4 m high, with nearly 40 m of usable test-section length. The achievable wind speeds in this section range from 0 to nearly 15 m/s, which is sufficient for most small aircraft. Detailed descriptions of the wind-tunnel facility are provided in a 2008 paper by Loxton et al. [5].

Turbulence levels in the wind engineering section of the tunnel can be controlled by changing the upper and lower tunnel configuration. Grids placed in the upper cross section are used to generate desired length scales of turbulence, while screens can be added in the upper and lower sections to reduce turbulence intensity. The jet and collector in the lower automotive test section have substantial effects on the turbulence levels in the upper section. By varying the configuration of screens, grids, jet, and collector, the wind tunnel can replicate turbulence measured in various outdoor environments [6]. These environments are representative of areas in which MAV operations are expected, ranging from relatively unobstructed fields to dense urban environments.

Turbulence levels in the tunnel are determined using a bank of four Cobra probes (Fig. 3), which measure three-component air velocities at 1250 Hz. The lateral spacing of the probes permits estimates of rolling or vortical gust features [6]. Such gusts contribute substantial disturbances to aircraft flight by generating spanwise variations in angles of attack that, in turn, generate roll moments and roll disturbances. The effects of such disturbances are quite large due to the typically fast roll dynamics of fixed-wing aircraft, which result from the aerodynamic roll damping and low roll moment of inertia [7–9].

B. Aircraft

The aircraft used in the wind-tunnel flight experiments is a commercially available recreational radio-controlled aerobatic design. The airframe structure comprises expanded polypropylene foam rigidized with embedded carbon-fiber spars and stringers. A straight, tapered wing with no dihedral is used with a symmetric airfoil and full-span ailerons, for which the chord is a relatively large percentage of the wing chord. Elevator and rudder surfaces are similarly proportioned, since the aircraft is designed for rapid maneuvering. The flying surface configuration is conventional, with a leading wing and trailing tail surfaces attached to the aft fuselage.

Foam aircraft structures, as in the test article, are useful for wind-tunnel flight tests where flight termination into obstacles is frequently expected during experiments. Expanded polypropylene foam is particularly well suited due to large structural elastic response to loads without material failure. The airframe is suitably rigid to withstand normal aerodynamic loads, yet it is sufficiently flexible to absorb impact energy and prevent or reduce airframe damage. In previous flight trials [5] in the turbulent wind tunnel, a large portion of the testing time was occupied by airframe and system repairs following crashes.

C. Instrumentation and Sensors

The aircraft is equipped with instrumentation, permitting the measurement of actuator position and aircraft response. The system is modular and uses separate devices for sensing, data measurements,

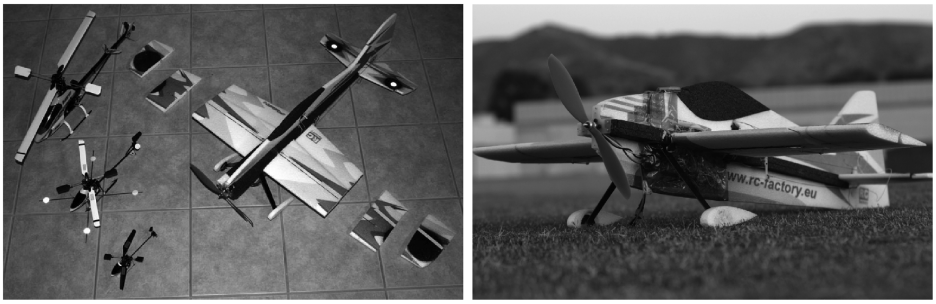

Fig. 2 Fixed-wing UAV shown with removable wingtip segments.

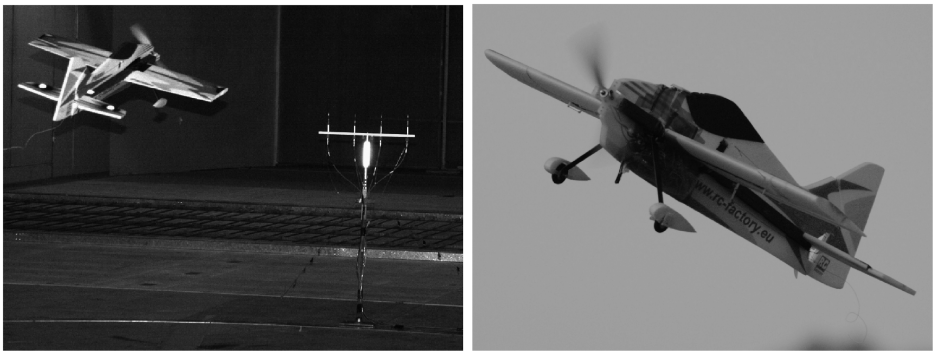

Fig. 3 Flight of configuration 1a behind the Cobra probes mounted in the wind-tunnel test section (left) and in open-air flight without air data measurement (right).

and data storage. The instrumentation is mounted to the exterior of the aircraft foam airframe on the left fuselage side underneath the wing, as in Figs. 2 and 3. An Atmel microcontroller (MCU) provides the overall system control, timing, and user interface [10]. The MCU requests samples from an analog-to-digital converter unit, which has 12-bit resolution and supports 16 analog input channels using a sequential multiplexer. Data frames are processed by the MCU and written to an onboard flash memory module. A sampling rate of 100 Hz is chosen to be sufficiently greater than the expected flight dynamics to capture the relevant piloted response and disturbance behavior.

Sensor units interface through wire harnesses to the data measurement unit. A triaxial linear accelerometer and two dual-axis angular rate sensors generate analog voltage outputs measured by the data board. Single-pole analog resistor-capacitor filters are used on each of the 16 input channels to filter noise and vibrations from the flight data measurements. A characteristic frequency of 5 Hz is used to permit measurement of relatively rapid responses while attenuating higher-frequency electrical noise and mechanical vibration induced by the propeller rotation. The choice of the filter characteristic frequency is based on the expected pilot input frequency and the associated aircraft dynamic rates.

Actuator position is determined for ailerons, elevator, and rudder control surfaces by measuring the analog voltage of the center pin on the position feedback potentiometers in each servomotor. This potentiometer is used internally for closed-loop position tracking and provides a convenient measurement of the output arm motion. Measurement of the actuator position is made without adversely affecting the operation of the servo. A linear conversion is used to map measured actuator position to control surface deflection.

D. Aircraft Configuration Variations

Parametric changes are made to the aircraft configuration to evaluate the resulting sensitivity to the replicated turbulence. Changes to the center of gravity, mass, and moment of inertia are made by relocating components or adding and redistributing masses on the airframe. Figure 3 illustrates the addition of flat, lead masses to the fuselage sides and upper wing roots. Changes to the wingspan and wing area are made by cutting outboard segments of the foam wing. The shortened wing experiments are performed with constant mass and also with constant wing loading. Table 1 summarizes the configuration changes made to the aircraft.

III. Flight Testing and Model Identification

A. Open-Atmosphere Flight Testing

The UAV is flight tested in the open atmosphere with negligible winds to identify a linear dynamic model for each configuration. Flight tests are conducted in a large, outdoor field that allows the aircraft to be trimmed and flown using standard flight-test maneuvers. These maneuvers perturb the aircraft about the trim condition and are used to identify both the control effectiveness and the flight dynamics. System identification techniques are used to estimate an

Table 1 Parametric configuration changes to fixed-wing UAV during wind-tunnel flight tests

Configuration	Description	Mass, kg	I_x, kg · m^2	I_y, kg · m^2	Span, m	Loading, kg/m^2
1a	40 cm span short	0.47	0.053	0.109	0.57	3.51
2a	20 cm span short	0.47	0.053	0.133	0.77	2.71
2b	20 cm span short + 135 g	0.61	0.061	0.134	0.77	3.46
3a	Standard	0.47	0.053	0.133	0.97	2.24
3b	100 g payload	0.57	0.059	0.134	0.97	2.69
3c	200 g payload	0.67	0.064	0.138	0.97	3.13
4a	Midroll/yaw MOI[a]	0.67	0.104	0.179	0.97	3.13
4b	High-roll/yaw MOI[a]	0.67	0.143	0.223	0.97	3.13

[a]MOI denotes moment of inertia.

equivalent model from the resulting flight data [11–13]. The estimated dynamics are used as a baseline for the characteristics of the vehicle at each configuration in the absence of turbulence.

The aircraft is excited about the trim using frequency sweep control inputs and control doublets performed on the aileron, elevator, and rudder commands. Model identification is performed using the frequency sweep inputs and tested for accurate estimation of the dynamics using the control doublets. Each of the control surface command sweeps are performed independently and repeated three times. Slow shifts in the mean stick position are made to keep the aircraft near the trim position. Cross-axis disturbance corrections are made with inputs dissimilar in frequency to the primary forcing. For instance, small elevator inputs are used during the aileron and rudder frequency sweeps to maintain the pitch trim of the aircraft throughout the maneuver. The dissimilar nature of the cross-axis inputs are designed to reduce contamination of the primary measurements [11].

Frequency sweeps and control doublets are flown manually using the control stick on the remote pilot's radio transmitter. Stick sensitivity during the maneuvers is configured such that full stick travel produces 20% of the total control surface movement. The reduced sensitivity facilitates maneuvering by helping the pilot maintain consistent, small control inputs. Initial sweep frequency is approximately 0.3 Hz and increases to about 4 Hz, which is near the limit of coordinated motion for the pilot.

The aircraft dynamics are assumed to be linear about the trimmed flight condition and invariant with time. Additionally, the lateral and longitudinal dynamics are assumed to be uncoupled. Equation (1) gives the general form of the dynamics in state-space representation, which includes contributions from state perturbations x, control inputs u, and external disturbances d. Identified dynamics are assumed to be free of external disturbances and are only modeled using a state matrix A and a control effectiveness matrix B. The disturbance response matrix E is described in Sec. IV and can take the form of either A or B, depending on the selection of the equivalent disturbances used in place of d:

$$\dot{x} = Ax + Bu + Ed, \qquad y = Cx \tag{1}$$

The assumed form of the lateral and longitudinal dynamics identified from the flight test are specified by Eqs. (2) and (3). The angular rotation states are directly measured, while the wind-axis orientation states are estimated using flight-path reconstruction techniques [13]:

$$\begin{bmatrix} \dot{\beta} \\ \dot{p} \\ \dot{r} \end{bmatrix} = \begin{bmatrix} Y_\beta & Y_p & Y_r \\ L_\beta & L_p & L_r \\ N_\beta & N_p & N_r \end{bmatrix} \begin{bmatrix} \beta \\ p \\ r \end{bmatrix} + \begin{bmatrix} Y_{\delta_a} & Y_{\delta_r} \\ L_{\delta_a} & L_{\delta_r} \\ N_{\delta_a} & N_{\delta_r} \end{bmatrix} \begin{bmatrix} \delta_a \\ \delta_r \end{bmatrix} \tag{2}$$

$$\begin{bmatrix} \alpha \\ q \end{bmatrix} = Cx_{\text{lon}} \begin{bmatrix} \dot{\alpha} \\ \dot{q} \end{bmatrix} = \begin{bmatrix} Z_\alpha & Z_q \\ M_\alpha & M_q \end{bmatrix} \begin{bmatrix} \alpha \\ q \end{bmatrix} + \begin{bmatrix} Z_{\delta_e} \\ M_{\delta_e} \end{bmatrix} [\delta_e] \tag{3}$$

The dynamics are identified using the output-error method, which estimates the lumped-parameter stability and control derivatives separately for the longitudinal- and lateral-direction equations of motion. Additional parameters in the observation equations are also estimated, allowing the model to predict lateral and vertical accelerations. Bias parameters are included in the estimation for both state and observation equations.

B. Turbulent Wind-Tunnel Flight Testing

Wind-tunnel tests consist of short duration flights where the pilot attempts to maintain straight-and-level attitude in the center of the test section. The pilot inputs are primarily used to reject attitude disturbances caused by turbulence and maneuver the aircraft to the center of the tunnel following a position disturbance.

Flights are initiated using a standard takeoff from the tunnel floor and are terminated by landing conventionally or, in some cases, by terminally impacting the tunnel walls or ceiling. Takeoffs are performed with some forward speed relative to the tunnel, then throttle is managed to maintain the aircraft in a fixed longitudinal position. Typical flight duration is about 120 s, with approximately 90 s of flight with the pilot attempting to maintain a stationary aircraft position within the tunnel.

All flight tests are performed with a fixed wind-tunnel speed of 8 m/s and a fixed wind-tunnel configuration, which results in an average turbulence intensity of 6.6%, with a length scale of 1.2 m. The wind tunnel is configured with the jet down, the collector in the forward position, no grids in the upper section, and two screens in the lower section [5]. The constant speed for the tests necessitates flight at varying trim angles of attack due to the change in mass for some configurations. Flight attempts at higher tunnel speeds and turbulence intensities (14%) were generally unsuccessful due to the severity of the disturbances and the correspondingly rapid departures from controlled flight. All flights at higher speeds and turbulence intensities ended with a terminal contact with the tunnel boundaries after a few seconds of attempted flight.

Figure 4 shows a short segment of flight data from wind-tunnel tests of two aircraft configurations. The left plot series shows the data from the standard aircraft configuration, with nominal weight and wingspan. The right plot series shows the results of adding a 100 g payload on each wingtip, which increases both the vehicle mass and the roll and yaw moments of inertia.

The data in Fig. 4 show only a short segment of each flight but depict trends that are consistent for each configuration. Disturbances acting on the heavier configuration (right plot) appear to have smaller amplitudes, particularly in vertical acceleration and roll rate. The control input magnitude remains relatively large for both cases, although the input frequency appears to be lower for the loaded case. Both the larger mass and moments of inertia contribute to a reduction in control effectiveness, so larger control inputs are necessary to generate aircraft responses. This is in agreement with the pilot

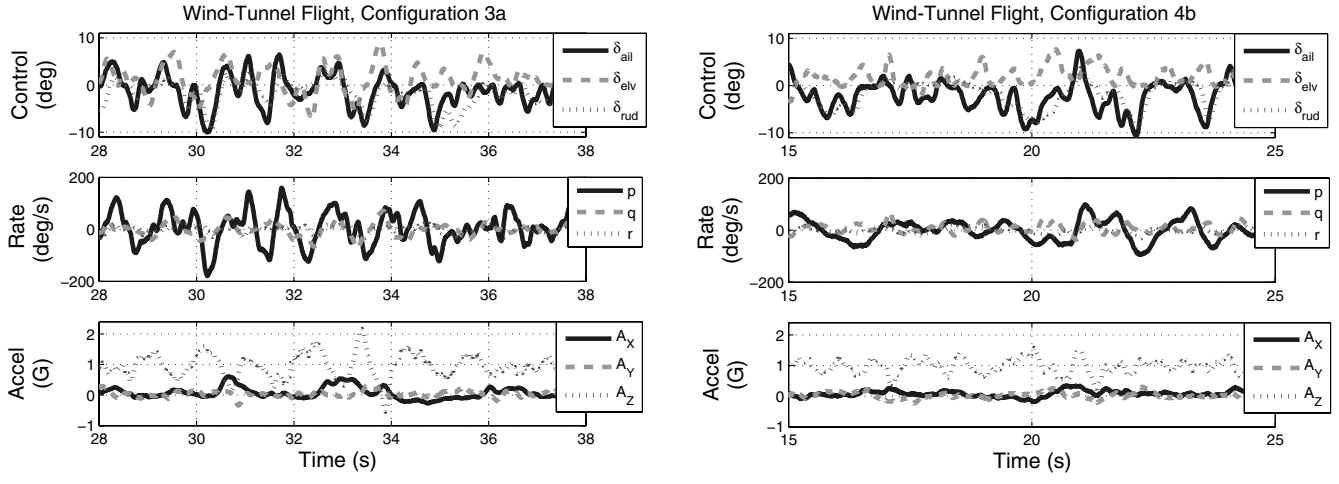

Fig. 4 Flight data measurements from attempted level flight with standard configuration 3a (left) and high-moment-of-inertia configuration 4b (right).

observations from the flight and is the obvious reason why the turbulent disturbances appear to be more benign. Increasing the inertia of the vehicle dampens the effect of the turbulent disturbances, in addition to reducing the response due to control inputs.

Wind-tunnel flight-test results in turbulence differ fundamentally from open-atmosphere flight data obtained in calm conditions, due to the constant and large amplitude disturbances acting on the vehicle in the former environment. Aircraft responses during open-air flights are assumed to strictly result from piloted control inputs, whereas responses in the wind tunnel are due to both inputs and disturbances. The maneuvering objectives of wind-tunnel tests are simply straight-and-level flight, so the piloted inputs consist entirely of recovery actions to prevent divergent attitude and position. The control inputs are always made in response to disturbances, since the aircraft could be conceivably trimmed to fly straight and level in the tunnel with no pilot input if it were not for the effects of the turbulence.

One measure of the relative contribution of turbulence to the aircraft response is in the computation of coherence between control surface input and aircraft response [14,15]. The coherence function gives a normalized estimate for the degree of linear relation between the controls and responses during flight tests. A coherence of one indicates that the output is linearly related to the input, as assumed by the state-space modeling in Eqs. (1–3). Conversely, a correlation of zero indicates that no linear relationship exists between the input and output, whether due to strong nonlinearity or due to the overwhelming presence of a disturbance to either measurement.

Equation (4) shows the computation of the frequency-dependent coherence function, $C_{io}(f)$, as a ratio of the square of the norm of the cross-spectral power density and the product of the input and output power-spectral densities. The subscript i denotes an input, such as aileron, elevator, or rudder, while the subscript o denotes an output, such as an angular rate or acceleration:

$$C_{io}(f) = \frac{|P_{io}(f)|^2}{P_{ii}(f)P_{oo}(f)} \tag{4}$$

Figure 5 shows the coherence function for both open-air flight test and wind-tunnel flight tests of two aircraft configurations. Upper plots show the coherence from open-air flight tests and lower plots show the results from the wind-tunnel tests. Standard aircraft configuration results are shown in the left plots, and high-payload-mass high-moment-of-inertia coherences are shown in the right plots.

The coherence functions in Fig. 5 show that the aircraft responses from open-air flight tests (upper plots) are linearly related to the piloted inputs for frequencies between 0 and 4 Hz. At larger frequencies, the coherence drops substantially. Piloted frequency sweeps are similarly bounded, so the high degree of coherence supports the linear modeling assumptions made during system identification. A notable exception is the rudder-to-lateral-acceleration coherence of the high-mass high-moment-of-inertia configuration (upper-right plot), which is somewhat low even in the piloted bandwidth. Coherence analysis of the standard aircraft configuration shows a linear input–output relation throughout the piloted bandwidth. The corresponding system identification shows good agreement between the measured data and the identified equivalent linear model. Open-air flight tests are conducted in open fields during negligible or mild wind and gust conditions, so the expected contributions of turbulence on the aircraft response are minimal. Conversely, the wind-tunnel flight tests are conducted in the presence of continuous high-intensity turbulence.

The lower two plots of Fig. 5 show the coherence functions computed from wind-tunnel flight tests. Compared with the open-air flight results, the wind-tunnel coherence is both lower in magnitude and decays more rapidly with increasing frequency. A substantial drop in coherence is evident at frequencies between 2 and 3 Hz for all data at all configurations. This region of low coherence may be related to the dominant turbulence length relative to the size of the aircraft, which causes a disturbance forcing at moderate frequencies. The coherence associated with the high-mass high-moment-of-inertia configuration at these frequencies is higher than the corresponding coherence for the standard configuration.

IV. Estimation of Turbulent Disturbances

A. Comparison of Predicted and Measured Aircraft Response

Forces and moments incurred in flight are computed using standard kinematic relations [9,11] and estimated inertial properties. Equation (5) shows the formulation for lateral and vertical forces and roll, pitch, and yaw moments in terms of the measured aircraft linear accelerations, angular rates, and estimated angular accelerations. The angular rotations are estimated using a filtered numerical center differencing [11]. A third-order Butterworth filter with a characteristic frequency of 15 Hz is applied bidirectionally to eliminate phase-lag effects of the filter and retain the numerical noise attenuating properties [16]. The subscript T is appended to the coefficients to indicate the total forces and moments, which may have component contributions from several sources:

$$C_{Y_T} = \frac{mA_y}{\bar{q}S}, \qquad C_{Z_T} = \frac{mA_z}{\bar{q}S}$$

$$C_{l_T} = \frac{I_x}{\bar{q}Sb}\left[\dot{p} - \frac{I_{xz}}{I_x}(pq + \dot{r}) + \frac{I_z - I_y}{I_x}qr\right]$$

$$C_{m_T} = \frac{I_y}{\bar{q}Sc}\left[\dot{q} + \frac{I_x - I_y}{I_y}pr + \frac{I_{xz}}{I_y}(p^2 - r^2)\right]$$

$$C_{n_T} = \frac{I_z}{\bar{q}Sb}\left[\dot{r} - \frac{I_{xz}}{I_z}(p - qr) + \frac{I_y - I_x}{I_z}pq\right] \tag{5}$$

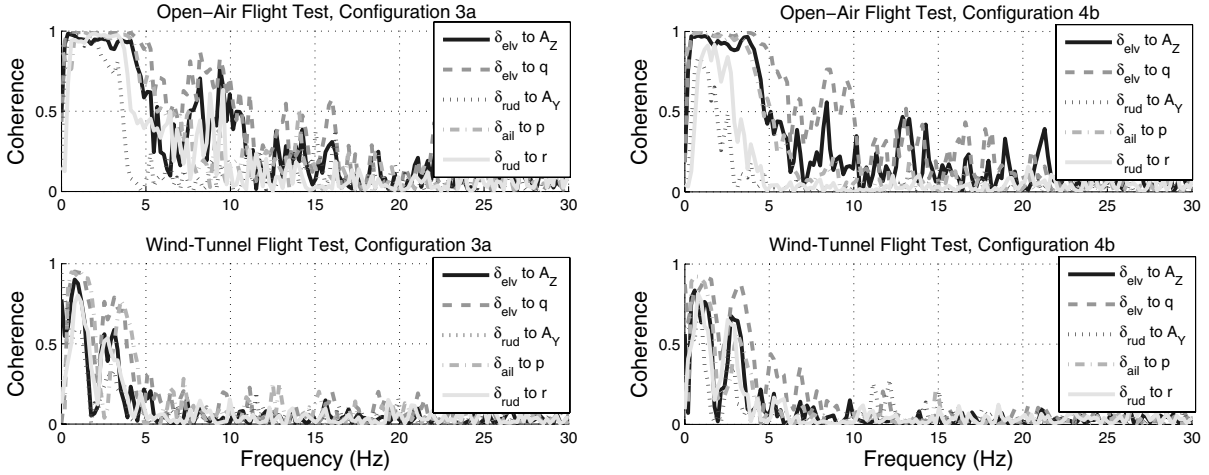

Fig. 5 Coherence between control inputs and aircraft responses for open-atmosphere flight tests (upper plots) and wind-tunnel flight tests (lower plots). Standard wing and mass configuration 3a (left plots) and high-mass high-moment-of-inertia configuration 4b (right plots).

Equation (5) uses the aircraft geometry and inertial reference quantities to nondimensionalize the forces and moments. The cross-axis responses are generally small compared with the primary axis, so the majority of the moments result from angular accelerations about the respective axis. Variations of the force and moment coefficients with time are computed by using the corresponding measurement and acceleration estimates from each data sample.

Appropriately dimensionalized, the force and moment coefficient estimates represent the actual forcing on the aircraft in flight. The sources of this forcing are due to aircraft damping, control deflections, or turbulent disturbances. Equation (6) shows the contributions of aircraft motion and control surface position to the forces and moments. The formulations specifically exclude the turbulent disturbances and assume that the aircraft is externally unforced. The subscript a is appended to the coefficients to indicate the forces and moments are due strictly to the aircraft components:

$$C_{Y_a} = C_{Y_\beta}\beta + C_{Y_r}\frac{b}{2V_0}r + C_{Y_{\delta_r}}\delta_r$$

$$C_{Z_a} = C_{Z_\alpha}\alpha + C_{Z_q}\frac{c}{2V_0}q + C_{Z_{\delta_e}}\delta_e$$

$$C_{l_a} = C_{l_\beta}\beta + C_{l_p}\frac{b}{2V_0}p + C_{l_r}\frac{b}{2V_0} + C_{l_{\delta_a}}\delta_a + C_{l_{\delta_r}}\delta_r$$

$$C_{m_a} = C_{m_\alpha}\alpha + C_{m_q}\frac{c}{2V_0}q + C_{m_{\delta_e}}\delta_e$$

$$C_{n_a} = C_{n_\beta}\beta + C_{n_p}\frac{b}{2V_0}p + C_{n_r}\frac{b}{2V_0} + C_{n_{\delta_a}}\delta_a + C_{n_{\delta_r}}\delta_r \quad (6)$$

Equation (6) estimates forces and moments from a known aircraft model, such as the one identified from open-air flight tests. Equations of motion in the form of Eqs. (2) and (3), where the states correspond to physical measurements, have elements that can be used directly in Eq. (6). Computation of the aircraft-predicted forces and moments amounts to a simulation of the identified dynamics model, which can be used with measured control deflections from flight, as are done with the wind-tunnel test data.

Turbulent disturbances can be estimated by comparing the total forces and moments from the aircraft flight with the predicted forces from the identified dynamic model. Equation (5) is used to generate estimates of two force and three moment coefficients for each aircraft response data frame. The forces and moments represent the sum of all forces acting on the vehicle, since they are estimated directly from the aircraft motion. Control input data corresponding to the aircraft motion are taken as input to the aircraft dynamics model identified in Eqs. (2) and (3). The output of the model is the predicted response of the vehicle due strictly to the inputs. These simulated outputs are used in Eq. (5) to estimate the forces and moments required to generate the predicted motion. Equivalently, estimated aircraft stability and control derivatives can be used to estimate the same forces using Eq. (6). The processes are essentially identical, except that the use of the aircraft parameter method offers visibility into the individual force contributions of responses and controls. In both cases, the simulated states of the aircraft dynamics are needed to compute the forces and moments predicted to act on the airframe. For a real-time implementation, the simulation can be akin to a reference model and used to generate a one-step prediction of the response.

Total forces and moments acting on the aircraft can be decomposed into contributions from the aircraft motion relative to fixed mass of air and the turbulent flow relative to a fixed aircraft. The simple relations are shown in Eq. (7) for the two forces and three moments:

$$C_{Y_T} = C_{Y_a} + C_{Y_d}, \qquad C_{Z_T} = C_{Z_a} + C_{Z_d}, \qquad C_{l_T} = C_{l_a} + C_{l_d}$$
$$C_{m_T} = C_{m_a} + C_{m_d}, \qquad C_{n_T} = C_{n_a} + C_{n_d} \quad (7)$$

B. Control Equivalent Turbulent Disturbance

Identifying the control equivalent to turbulence gives direct insight into the control effort required to negate the effect of the disturbances. The process identifies the combination of control surface deflections that, in the absence of turbulence, would result in the same aircraft response. In particular, the forces and moments imparted by the unsteady air movements are used to find the control deflections that produce the same forces on the aircraft structure due to changes in camber. Control equivalent turbulent disturbances (CETDs) are typically used in simulation environments as a means of generating a physically significant turbulence model [17]. In the current context, a CETD is used to define estimated turbulence acting on a flight vehicle in terms of available control authority.

Equivalent control deflections are computed by using a pseudo-inverse control allocation approach [18], where the forces and moments from the measured aircraft response are taken as the desired acceleration vector. The process is identical to a least-squares linear regression [14], except that control allocation includes an additional weighting matrix to represent actuation limits. The known control effectiveness coefficients from Eq. (6) identify the force and moment sensitivity from each control surface. The pseudoinverse method finds a solution to the unknown control deflection vector necessary to generate the desired accelerations using the available control effectors. Equation (8) shows the general form of control equivalent turbulence disturbances for state-space systems:

$$C_d = B\delta_d \quad (8)$$

Here, C_d is the vector of forces and moments computed from measurements, B is the control effectiveness matrix, and δ_d is the vector of equivalent control inputs. Equation (9) gives an expanded form for typical aircraft parameters:

$$\begin{bmatrix} C_{Y_d} \\ C_{Z_d} \\ C_{l_d} \\ C_{m_d} \\ C_{n_d} \end{bmatrix} = \begin{bmatrix} 0 & 0 & C_{Y_{\delta_r}} \\ 0 & C_{Z_{\delta_e}} & 0 \\ C_{l_{\delta_a}} & 0 & C_{l_{\delta_r}} \\ 0 & C_{m_{\delta_e}} & 0 \\ C_{n_{\delta_a}} & 0 & C_{n_{\delta_r}} \end{bmatrix} \begin{bmatrix} \delta_{a_d} \\ \delta_{e_d} \\ \delta_{r_d} \end{bmatrix} \quad (9)$$

Cross-axis control derivative terms, which are typically small for conventional aircraft geometries, are assumed to be zero. The primary control actions $C_{l_{\delta_a}}$, $C_{m_{\delta_e}}$, and $C_{n_{\delta_r}}$ are shown along the lower diagonal of the moment effectiveness submatrix. The ailerons are assumed to use equal and opposite deflections on opposing wings, such that they generate no vertical force or pitching moment effects.

The control allocation approach using conventionally grouped control surfaces works well for strictly generating desired moments, but it may not converge to an adequate solution for cases that require independent forces and moments. Elevator, for instance, affects both vertical force and pitch moment, but does so in a coupled manner that precludes independent control of either.

Aileron actuation on UAVs is often achieved using an electromechanical actuator embedded into the wing surface forward of each of the two aileron surfaces. The use of two aileron actuators eliminates the need for pulleys, cables, pushrods, and bellcranks in the wing surface, but it also allows the two aileron surfaces to move independently. Standard aileron action is achieved by actuating differentially, and a flaplike action can be achieved by commanding the actuators collectively. Each of the two aileron segments can be treated as an independent control effector, which allows contributions to the vertical force and pitching moment. With a modified control effectiveness matrix, the pseudoinverse control allocation approach is able to achieve independent control of the longitudinal states [9,19]. Independent control of lateral forces and moments (in particular, side force and yaw moment) can be conceivably achieved by the addition of a forward vertical stabilizer [20].

Equation (10) gives the equivalent control disturbance result for independent ailerons $\delta_{a,r}$ and $\delta_{a,l}$ for the right and left ailerons, respectively:

$$\begin{bmatrix} C_{Y_d} \\ C_{Z_d} \\ C_{l_d} \\ C_{m_d} \\ C_{n_d} \end{bmatrix} = \begin{bmatrix} 0 & 0 & 0 & C_{Y_{\delta_r}} \\ C_{Z_{\delta_{a,r}}} & C_{Z_{\delta_{a,l}}} & C_{Z_{\delta_e}} & 0 \\ C_{l_{\delta_{a,r}}} & C_{l_{\delta_{a,l}}} & 0 & C_{l_{\delta_r}} \\ C_{m_{\delta_{a,r}}} & C_{m_{\delta_{a,l}}} & C_{m_{\delta_e}} & 0 \\ C_{n_{\delta_{a,r}}} & C_{n_{\delta_{a,l}}} & 0 & C_{n_{\delta_r}} \end{bmatrix} \begin{bmatrix} \delta_{a,r_d} \\ \delta_{a,l_d} \\ \delta_{e_d} \\ \delta_{r_d} \end{bmatrix} \tag{10}$$

Rejecting turbulent disturbances essentially requires commanding the control effectors directly in opposition to the equivalent control deflections. The forces and moments imparted on the aircraft by the turbulent flow are then exactly opposed by the control surfaces. This concept is somewhat notional given the inherent phase delay associated with sensing a disturbance before it can be rejected.

CETDs are computed using the effectiveness of the various surfaces but irrespective of the actuators that drive them. Equivalent control deflections are determined for each time increment of measured aircraft response, so solutions are not affected by measurements adjacent in time. Frequency content in the equivalent control deflections over some time period are limited only by the Nyquist frequency of the sampling rate rather than by the dynamic model of the actuators. Furthermore, the control allocation process may yield equivalent deflections that are outside the position limits of the actuator. Practical use of the approach for disturbance rejection must be within the bounds of the actuator bandwidth.

C. Equivalent Disturbance Sensitivity of Aircraft Configurations

Figure 6 shows power-spectral density of estimated turbulence (left) and control equivalent turbulence (right) from a 40 s time history of flight near the center of the wind tunnel for variable-mass configurations. The standard aircraft configuration (3a) is compared against increases of 100 g (3b) and 200 g (3c). Both lateral force C_Y and vertical force C_Z show the expected trend of decreased disturbance sensitivity with increased mass. Variations in the moment disturbances are not consistent with mass changes.

Elevator control power between frequencies of 0.4 to 3 Hz decreases with increasing mass and inertial stiffness. Since the weight is added at the c.g., it is possible that the stabilizing influence is due to a coupled effect where the vertical acceleration perturbations are reduced and, in turn, cause a reduction in the pitching disturbances. This resulting effect on the pitching moment sensitivity to increasing mass is evident in the right center plot, which shows the equivalent elevator disturbance decreases in variance with mass.

Equivalent aileron and elevator powers remain high to nearly 3 Hz, while rudder power becomes noticeably attenuated at frequencies greater than 1 Hz. This disparity is consistent with pilot observations, noting higher workload in roll and pitch axes, which may be a characteristic of the replicated turbulence flow. Equivalent aileron and rudder trends are not consistent with mass.

Figure 7 shows the power-spectral density trends with increasing wing area and fixed-wing loading for turbulence forces (left) and equivalent control deflections (right). All estimated turbulence quantities apart from pitching moment exhibit decreasing power with increasing wing area. The force bandwidth decreases with wing area, matching the pilot observation that the larger configurations exhibit damped responses. Conversely, the short-wing configuration (1a) shows a rapid departure tendency and increased pilot workload. The moment disturbances show higher-frequency content compared with the forces, although the trends in decreasing bandwidth with increasing wingspan are also evident.

Large-magnitude lateral disturbances, particularly side force, contribute to large equivalent rudder deflection over a wide range of frequencies. The middle- and long-wingspan cases (respectively, 2b and 3c) show significantly less equivalent rudder disturbance. Equivalent elevator deflections show decreasing magnitudes at low and intermediate frequencies with respect to increasing wingspan, whereas equivalent aileron does not show a trend that is consistent with wingspan variations.

Figure 8 shows the frequency content of estimated turbulence forces and moments (left) and of CETD (right) for configurations with varying wing area and fixed mass. Moments C_l, C_m, and C_n show power decreases with increasing wingspan, although the trend is reversed in C_m for frequencies between 0.5 to 1.1 Hz. Similarly, trends in turbulence forces C_Y and C_Z are not consistent with wingspan changes. Large C_Y and C_n magnitude for configuration 1a

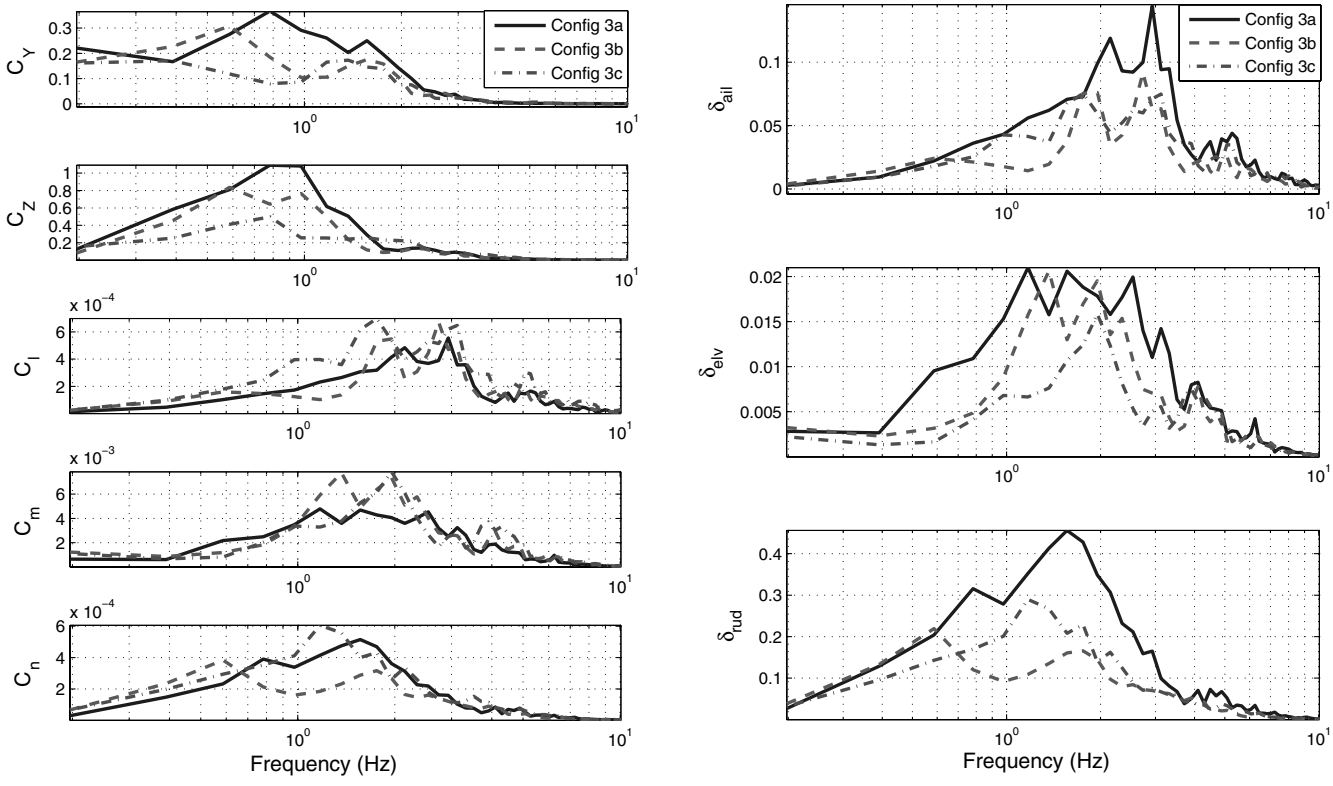

Fig. 6 Power-spectral density of turbulence forces and moments (left) and CETD (right) for variable-mass constant wingspan configurations 3a, 3b, and 3c.

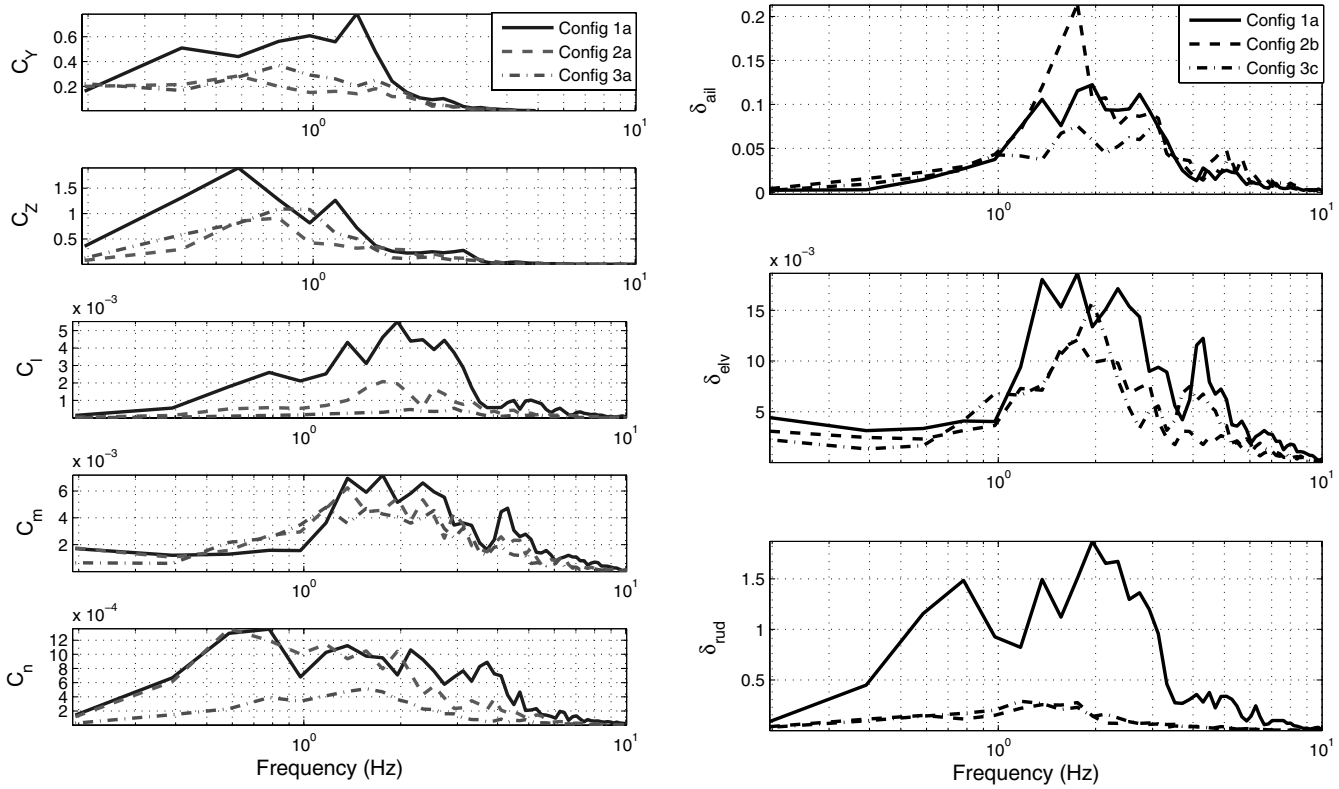

Fig. 7 Power-spectral density of turbulence forces and moments (left) and of CETDs (right) for variable wing area, constant wing-loading configurations 1a, 2b, and 3c.

causes the equivalent rudder to exhibit large-amplitude deflection at intermediate frequencies. Such an effect could be explained by the reduction in the yaw stabilizing influence of the wing, which increases with span. However, the intermediate wingspan case (2a) does not reflect the larger equivalent rudder deflection compared with the nominal case (3a).

Equivalent elevator deflections at low frequencies increase with span, an effect perhaps caused by the change in relative areas of the

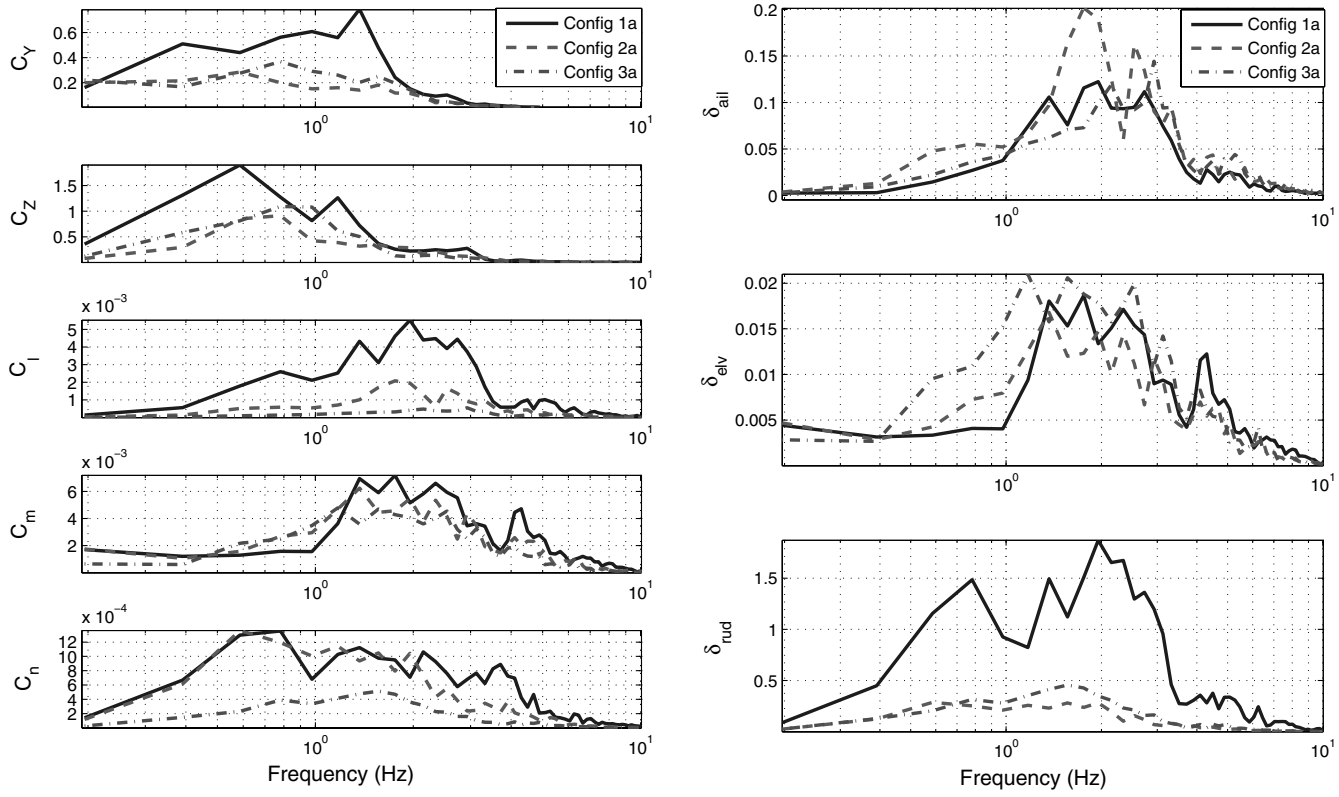

Fig. 8 Power-spectral density of estimated turbulence forces and moments (left) and of CETDs (right) for variable wing area, constant mass configurations 1a, 2a, and 3a.

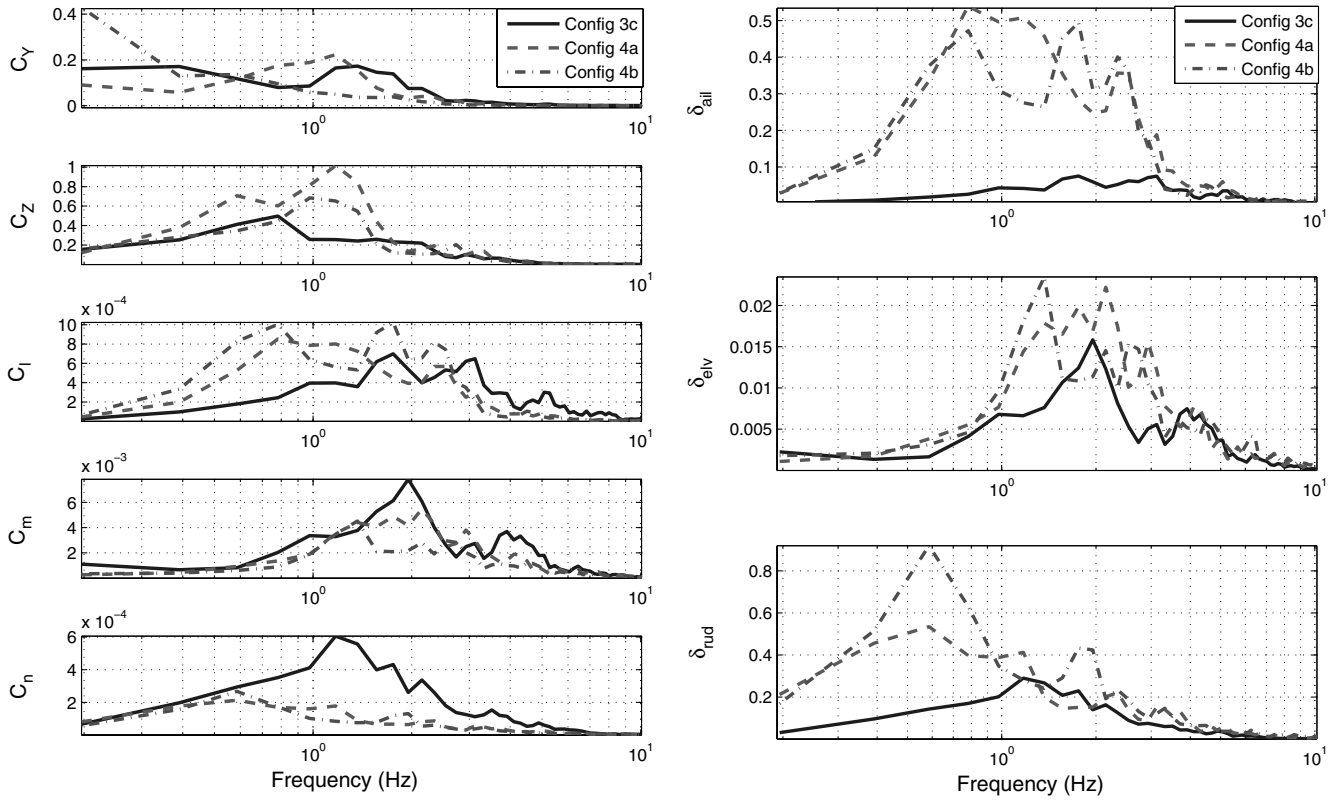

Fig. 9 Power-spectral density of estimated turbulence forces and moments (left) and of CETDs (right) for variable roll and yaw moment of inertia configurations 3a, 4a, and 4b.

horizontal stabilizer and the wing, causing increased pitch trim and pitch damping authority for the short-wing configuration (1a). At higher frequencies, the equivalent elevator results are not clearly correlated with span variation.

The pilot reported notably increased roll sensitivity with decreasing span for the configuration sets shown in Figs. 7 and 8. The aircraft appeared more likely to be disturbed in roll, although the vehicle responded more promptly to control input. The combined effects produced no changes in the equivalent aileron deflection, since the tendency toward divergence is opposed by the increased control effectiveness of decreasing wing area and wingspan.

Figure 9 shows the estimated turbulence (left) and CETD (right) variation with increasing roll and yaw moments of inertia. Equivalent aileron deflection increases with roll moment of inertia, which is caused by the increased roll stiffness, decreased aileron control effectiveness, and reduced sensitivity to disturbances. The increased equivalent aileron requirement occurs only at low to moderate frequencies, where the inertial stiffness is of relatively little consequence. All configurations have similar aileron requirements at high frequencies, where roll disturbances cause significant roll accelerations. The pilot feedback on the handling qualities indicated that the higher-inertia configurations required less rapid, yet larger magnitude, stick inputs.

Table 2 Fit quality of longitudinal- and lateral-system identification for each configuration determined from Eq. (11)

Configuration	A_y	A_z	p	q	r
1a	0.2	0.2	0.1	0.1	0.3
2a	0.3	0.1	0.1	0.1	0.2
2b	0.3	0.2	0.1	0.1	0.2
3a	0.3	0.1	0.1	0.1	0.3
3b	0.3	0.1	0.1	0.1	0.3
3c	0.2	0.1	0.1	0.1	0.2
4a	0.3	0.1	0.1	0.1	0.3
4b	0.3	0.1	0.1	0.1	0.3

Larger equivalent rudder amplitude is required due to the decreased rudder effectiveness, particularly at low frequencies. The rudder deflection requirement shows a smaller increase than equivalent aileron for increasing moment of inertia. Such an effect could be a combination of the differences between weathercock and roll convergence dynamics and could also be affected by the nature of the wind-tunnel flow, which is more prone to axial flow disturbances.

Increasing roll and yaw moments of inertia results in increased roll moment disturbances at low frequency and decreased disturbances at high frequency. Yaw disturbances decrease with inertia over the tested frequency range. Some effect on the force disturbances is evident, although it remains inconsistent with inertia.

D. Uncertainty in the Determination of Equivalent Turbulent Disturbances

Estimating CETDs is subject to a number of error sources. Both bias and random errors in the sensor measurement can propagate to erroneous estimates of the total forces. Force coefficient estimates are subject to additional error due to the inertial and reference parameters of the aircraft, for which the values may be uncertain. Additionally, the measured control inputs are used as input to an imperfect model of the aircraft dynamics, for which the outputs are subject to the prediction error given in Table 2. The parameter identification process includes a flight-path reconstruction step that includes the estimate of angle-of-attack and sideslip time histories. Since the wind-orientation derivatives are identified using the corresponding state time histories, errors in the flight-path reconstruction can propagate to uncertainty in the derivatives. Gyroscope and accelerometer scale factor and bias errors are partly corrected during the reconstruction procedure, although the lack of angle-of-attack and sideslip measurements preclude full sensor error correction.

The relative motion approach of aircraft with respect to air and turbulence with respect to aircraft depends on the validity of linear superposition, which in practice is acceptable for small maneuvers but may degrade the fitness of the estimate for highly dynamic maneuvers where aerodynamic nonlinearity may occur. The

assumption of axes separation in the identified dynamics may be unrealistic, as the maneuvers used for identification are generally small-amplitude frequency sweeps and doublets performed on control axes individually. Wind-tunnel flights include large control deflections made simultaneously to lateral and longitudinal axes, which may introduce coupling effects that are not considered in the system identification. The effect of these errors, whether individually or collectively, is expected to cause some uncertainty in the estimates of the turbulent forces and moments.

The final step in the computation of CETD is the dynamic inversion, which uses the identified control effectiveness matrix to approximate the control deflection required to achieve the estimated turbulent forces and moments at each time instant. The uncertainty associated with the control derivatives affects the estimate for the equivalent deflections, in addition to the aforementioned predicted response.

Stability and control derivatives are estimated using a maximum-likelihood output-error process, which iterates on the state and output equations to find the set of parameters that minimizes the difference between the simulated and measured responses. The method computes a gradient and determines both the parameter step for each iteration and a corresponding standard deviation, which approximates the estimation uncertainty. Relative standard deviation values are generally low (0–10%) for primary-axis derivatives, such as C_{l_p} or $C_{m_{\delta_a}}$, but they are higher for offaxis derivatives. Some derivatives that are nominally zero can have large relative standard deviation values (20–50%), although the effect on the output remains low due to the small influence in the state and output equations.

The kinematic equations used to compute the forces and moment are exact, although practical use will result in error due to imperfect measurements. The bias and scale factor error correction applied in the flight-path reconstruction process helps reduce the error in the force and moment computed from kinematics. The forces and moments computed from the predicted response are subject to several additional error sources, including parameter accuracy and the assumption of linearity during large amplitude, combined control inputs. and aircraft responses.

The quality of the identified model is assessed using Theil's inequality coefficient, in Eq. (11), which assigns a value representing the agreement between the simulated output and the measured output. A fit of 0.0 indicates an exact match between the data. Considering the noise in the sensor measurements and possible unmodeled dynamics, a fit value of 0.3 and below is considered acceptable [13]:

$$\text{fit} = \frac{\sqrt{\frac{1}{N}\sum_{k=1}^{N}[z(k)-y(k)]^2}}{\sqrt{\frac{1}{N}\sum_{k=1}^{N}z(k)^2}+\sqrt{\frac{1}{N}\sum_{k=1}^{N}y(k)^2}} \tag{11}$$

Vertical acceleration, roll rate, and pitch rate states are identified with excellent agreement to the flight measurements, while lateral acceleration and yaw rate show large errors. Cross-axis derivatives between aileron input and directional response primarily contributed to the errors. Time-history plots of the simulated system show the maximum prediction error is roughly less than 30% of the peak response for the offaxis responses, while the error remains within 10% for all primary axes. Directional responses to rudder actuation, for instance, show excellent agreement.

The prediction errors limit the admissibility of derived turbulence and CETD values in comparing the responses of the aircraft configurations. The trends illustrated show effects that provide physical insight into the sensitivity of aircraft design parameters, although improved parameter identification can result in more meaningful numerical results. In practical application, the derived disturbance estimates can provide a beneficial early response to turbulence as a feedforward command to the control surfaces. The aircraft response may be improved relative to a feedback-only approach, even if the equivalent control deflection contains some error.

V. Conclusions

The current research presents an analysis of an aircraft flown in replicated turbulence with varying geometry and inertial configuration. Open-air flight tests and identification of the aircraft dynamics are used to establish a baseline for the predicted performance of an aircraft configuration. The aircraft is then flown untethered in a turbulent wind tunnel, where the disparity between the predicted and measured behavior is used to estimate the forces and moment due to turbulence acting on the aircraft. These forces and moments can be expressed as equivalent control deflections, which afford insight into the practical effect of the disturbances on the aircraft control.

Comparisons of the various control configurations revealed known tradeoffs, such as the beneficial effects of aircraft mass and wing loading on attenuating force disturbances. Other results were less obvious, such as the influence of the roll moment of inertia on the equivalent aileron requirement, where the increased moment of inertia resulted in an increased equivalent aileron despite the effects of inertial roll stiffness.

Increased wing area caused a decrease in the low-frequency equivalent elevator with constant wing loading, but it resulted in increased elevator with constant mass. For the constant mass configurations, the decrease in wing loading that accompanied an increase in wing area contributed to the pitch divergence tendency at low frequencies. Interestingly, in all other metrics apart from pitch, the reduced wing loading appeared to decrease the influence of turbulence on the aircraft. It was the smaller, more heavily loaded configuration that was the most sensitive.

The results fall short of defining the ideal aircraft design for high-turbulence environments, but they demonstrate the sensitivity of classical aircraft sizing parameters on the response to turbulent disturbances. The configurations less affected by disturbances can be taken as approximate guidelines for preliminary designs of new UAVs. Alternatively, the more sensitive configurations can be used as benchmarks to test closed-loop disturbance rejection strategies, for which the aim may be to exploit performance benefits while mitigating inherent turbulence sensitivity.

Acknowledgments

The funding for this research was provided by the U. S. Air Force Office of Scientific Research/Asian Office of Aerospace Research and Development. The authors would like to thank the colleagues who devoted substantial effort in providing assistance with the research. The operators of the Monash wind tunnel were courteous and accommodating during the wind-tunnel flight trials. Tasneem Koleilat assisted throughout the wind-tunnel and flight testing in data recording, photography, and hardware repairs. Sridhar Ravi, Mark Thompson, and Edward Cruz of RMIT University supported the flight experiments and tunnel preparation. Mark Thompson also contributed the tunnel flight photograph. Troy Wigton provided the photograph of the aircraft in open-air flight.

References

[1] Reymer, D. P., *Aircraft Design: A Conceptual Approach*, 4th ed., AIAA, Reston, VA, 2006.

[2] Jenkins, D., Ifju, P., Abdulrahim, M., and Olipra, S., "Assessment of Controllability of Micro Air Vehicles," *Proceedings of the 16th Bristol International RPV/UAV Conference*, 2001.

[3] Raney, D., Cabell, R., Sloan, A., Hautamaki, B., Barnwell, W., and Lion, S., "Wind Tunnel Test of an RPV with Shape-Change Effector and Sensor Arrays," AIAA Guidance, Navigation, and Control Conference, AIAA Paper 2004-5114, Aug. 2004.

[4] Waszak, M. R., and Srinathkumar, S., "Flutter Suppression for the Active Flexible Wing—Control System Design and Experimental Validation," AIAA Dynamics Specialists Conference, AIAA Paper 1992-2097, April 1992.

[5] Loxton, B., Abdulrahim, M., and Watkins, S., "An Investigation of Fixed and Rotary Wing MAV Flight in Replicated Atmospheric Turbulence," 46th AIAA Aerospace Sciences Meeting, AIAA Paper 2008-227, Jan. 2008.

[6] Watkins, S., Milbank, J., Loxton, B., and Melbourne, W., "Atmospheric Winds and Their Implications for Micro Air Vehicles," *AIAA Journal*,

Vol. 44, No. 11, 2006, pp. 2591–2600.
doi:10.2514/1.22670

[7] Nelson, R. C., *Flight Stability and Automatic Control*, 2nd ed., McGraw–Hill, New York, 1998.

[8] Stevens, B. L., and Lewis, F. L., *Aircraft Control and Simulation*, 2nd ed., Wiley, New York, 2003.

[9] Etkin, B., *Dynamics of Atmospheric Flight*, Dover, New York, 2005.

[10] Barret, S. F., and Pack, D. J., *Atmel AVR Microcontroller Primer: Programming and Interfacing*, Morgan and Claypool Publ., San Rafael, CA, 2008.

[11] Klein, V., and Morelli, E. A., *Aircraft System Identification: Theory and Practice*, AIAA, Reston, VA, 2006.

[12] Ljung, L., *System Identification Theory for the User*, Prentice–Hall, Upper Saddle River, NJ, 1999.

[13] Jategaonkar, R. V., *Flight Vehicle System Identification: A Time Domain Methodology*, AIAA, Reston, VA, 2006.

[14] Bendat, J. S., and Piersol, A. G., *Random Data: Analysis and Measurement Procedures*, Wiley–Interscience, New York, 2000.

[15] Stoica, P., and Moses, R., *Introduction to Spectral Analysis*, Prentice–Hall, Upper Saddle River, NJ, 1997. pp. 61–64.

[16] Oppenheim, A. V., and Schafer, R. W., *Discrete-Time Signal Processing*, Prentice–Hall, Upper Saddle River, NJ, 1989.

[17] Lusardi, J., Blanken, C., and Tischler, M., "Piloted Evaluation of a UH-60 Mixer Equivalent Turbulence Simulation Model," *American Helicopter Society 59th Annual Forum* [CD-ROM], American Helicopter Society, Alexandria, VA, 6–8 May 2003.

[18] Oppenheimer, M. W., Doman, D. B., and Bolender, M. A., "Control Allocation for Over-Actuated Systems," *IEEE Control and Automation, 2006: 14th Mediterranean Conference on Volume*, IEEE Publ., Piscataway, NJ, June 2006, pp. 1–6.

[19] Sachs, G., "Predictor-Tunnel Display and Direct Force Control for Improving Flight Path Control," AIAA Guidance, Navigation, and Control Conference, AIAA Paper 2008-6644, Aug. 2008.

[20] Chatterjee, S., Lind, R., Roberts, B., and Gedeon, A., "Pterodactyl-Inspired Unpiloted Air Vehicle with Multimodal Locomotion," *2008 Joint Meeting of the Geological Society of America*, Houston, TX, Nov. 2008.